

Cloud Detection with MODIS, Part I: Improvements in the MODIS Cloud Mask for Collection 5

\*Richard A. Frey, Steven A. Ackerman, Yinghui Liu, Kathleen I. Strabala, Hong Zhang,

Jeffrey R. Key and Xuangi Wang

Cooperative Institute for Meteorological Satellite Studies, University of Wisconsin-Madison

1225 W. Dayton St. Madison, WI, USA 53706-1612

\* Corresponding author address:

Richard A. Frey

CIMSS

University of Wisconsin-Madison

1225 W. Dayton St.

Madison, WI 53706

e-mail: [Richard.frey@ssec.wisc.edu](mailto:Richard.frey@ssec.wisc.edu)

August 2007

## ABSTRACT

Significant improvements have been made to the MODIS cloud mask (MOD35 and MYD35) for Collection 5 reprocessing and forward stream data production. Most of the modifications are realized for nighttime scenes where polar and oceanic regions will see marked improvement. For polar night scenes, two new spectral tests using the 7.2  $\mu\text{m}$  water vapor absorption band have been added as well as updates to the 3.9-12  $\mu\text{m}$  and 11-12  $\mu\text{m}$  cloud tests. More non-MODIS ancillary input data has been added. Land and sea surface temperature maps provide crucial information for middle and low-level cloud detection and lessen dependence on ocean brightness temperature variability tests. Sun-glint areas are also improved by use of sea surface temperatures to aid in resolving observations with conflicting cloud vs. clear-sky signals, where visible and NIR reflectances are high, but infrared brightness temperatures are relatively warm. Day and night Arctic cloud frequency results are compared to those created by the Extended AVHRR Polar Pathfinder (APP-X) algorithm. Day versus night sea surface temperatures derived from MODIS radiances and using only the MODIS cloud mask for cloud screening are contrasted. Frequencies of cloud from sun-glint regions are shown as a function of sun-glint angle to gain a sense of cloud mask quality in those regions. Continuing validation activities are described in Part II of this paper.

## 1. MODIS Cloud Mask Overview

The MODIS (Moderate Resolution Imaging Spectroradiometer) is a key instrument of the Earth Observing System (EOS). It measures radiances at 36 wavelengths including infrared and visible bands with spatial resolution 250 m to 1 km. Earth Observing System models require knowledge of whether a radiance profile is cloud free. If the profile is not cloud free, it is valuable to have information concerning the type of cloud. Cloud mask algorithms for MODIS that use a series of sequential tests on the radiances or their associated brightness temperatures, may be found in Ackerman et al. (1998), King et al. (2003), and Platnick et al, (2003) where their description as part of the MODIS Cloud Products Suites is described.

Cloud detection is based on the contrast (i.e., cloud vs. background surface) in a given target area; in this case, a 1-km (at nadir) pixel. Contrast may be defined as differing signals for individual spectral bands (e.g. clouds are generally more reflective in the visible but colder than the background as measured in the thermal IR), spectral combinations (e.g. 0.86/0.66  $\mu\text{m}$  ratio is close to unity for cloudy skies), or temporal and spatial variations of these. The MODIS cloud mask uses several cloud detection tests to indicate a level of confidence that MODIS is observing a clear sky scene. Produced for the entire globe, day and night, and at 1-km resolution, the cloud mask algorithm employs up to fourteen MODIS spectral bands (250-m and 500-m band radiances aggregated to 1-km) to maximize reliable cloud detection. In addition, a 250-m mask derived from the two 250 m resolution bands (0.65 and 0.86  $\mu\text{m}$ ) in combination with 1-km cloud mask results is produced and archived, but will not be discussed here. The 1-km mask is independent of the 250-m mask.

The cloud mask assesses the likelihood that clouds obstruct a given pixel. As cloud cover can occupy a pixel to varying extents, the MODIS cloud mask is designed to allow for varying degrees of clear sky confidence, i.e., it provides more information than a simple yes/no decision. To assist users in interpreting the results, the cloud mask consists of 48 bits of output per pixel that includes information on individual cloud test results, the processing path, and ancillary information (e.g., land/sea tag). In addition, the first 8 bits of the cloud mask provide a summary adequate for many processing applications. Further, the first two bits of the mask summarize the results from all individual tests by classifying cloud contamination in every pixel of data as either *confident clear*, *probably clear*, *uncertain/probably cloudy*, or *cloudy*.

The MODIS cloud mask algorithm identifies several conceptual domains according to surface type and solar illumination including land, water, snow/ice, desert, and coast for both day and night. Once a pixel is assigned to a particular domain (defining an algorithm path), a series of threshold tests attempts to detect the presence of clouds or optically thick aerosol in the instrument field-of-view. Each test returns a confidence level that the pixel is clear ranging in value from 1 (high confidence clear) to 0 (very low confidence clear or high confidence of cloud or other obstruction). Ackerman et al. (1998) provides details of confidence calculations for individual spectral tests. There are several types of tests, where detection of various cloud conditions relies on different sets of tests. Those capable of detecting similar cloud conditions are grouped together. While these groups are arranged so that independence between them is maximized; few, if any, spectral tests are completely independent. As described by Ackerman et al. (1998), a minimum confidence is determined for each group as follows:

$$G_{j=1-N} = \min[F(i,j)]_{i=1-m}, \quad (1)$$

where  $F_{i,j}$  is the confidence level of an individual spectral test,  $m$  is the number of tests in a given group,  $j$  is the group index, and  $N$  is the number of groups (e.g. 5). The final cloud mask confidence ( $Q$ ) is then determined from the products of the results for each group,

$$Q = \sqrt[N]{\prod_{i=1}^N G_j}. \quad (2)$$

The four confidence levels included in the cloud mask output are: (1) *confident clear* ( $Q > 0.99$ ); (2) *probably clear* ( $Q > 0.95$ ); (3) *uncertain/probably cloudy* ( $Q > 0.66$ ); and (4) *cloudy* ( $Q \leq 0.66$ ). These outcomes constitute bits 1 and 2 of the mask. Note that the result gives the confidence, or lack thereof, in the existence of a clear pixel and not the confidence in the presence of an overcast cloudy pixel. As such, the *cloudy* outcome can alternately be labeled as *not clear* (i.e., high confidence in an obstruction in the field of view).

This approach is clear-sky conservative in the sense that if any test is highly confident that a scene is cloudy ( $F_{i,j} = 0$ ), the final clear sky confidence is also 0. However, it is also the case that the overall mask cannot be clear-sky conservative if individual test thresholds are set to flag only thick cloud or overcast conditions. Therefore, thresholds are set so that they detect the maximum number of cloudy pixels without generating unacceptably large number of “false alarms” (clear pixels incorrectly flagged as cloudy). Though an attempt has been made to represent regional and global cloud fractions by aggregating pixels flagged as either cloudy or probably cloudy, we recognize that some users may need more detail. For example, a reasonably accurate estimate of high cloud frequency may be obtained by counting only those pixels for which high cloud tests are positive. Much detailed information is contained in Ackerman, et al. (2006) and the MODIS Cloud Mask User’s Guide available at <http://cimss.ssec.wisc.edu/modis1/pdf/CMUSERSGUIDE.PDF>.

## 2. Cloud Mask Enhancements

### *a. Polar Night*

Discriminating clear sky from cloudy conditions is nowhere more difficult than in conditions of polar night. Also, verifying cloud detection results in polar night conditions is very difficult without human observations or active sensors to compare with. Both are almost totally absent during polar winter. Figure 1 shows both the underlying problem in cloud detection for polar night and an indication of cloud mask results. It shows a histogram of observed BTs from one MODIS granule (open bars) over frozen ocean near the North Pole. Also shown are the amounts of confident clear and confident cloudy retrievals for each BT class. Instead of clear-sky observations making a distinct peak on the warm end of the histogram as in most Earth scenes, this shows a more Gaussian distribution with most values (both clear and cloudy) somewhere in the middle. However, as shown in the figure, in a given region one expects temperatures and water vapor loading in clear skies over the surface ice to be relatively uniform so that a majority of those BTs will fall in one 5K-wide class. This was verified by inspection of the imagery for this granule. Note that many, if not most of the confident cloudy BTs were in either the same or warmer BT classes as that of the clear-sky peak, indicating the lack of thermal contrast that is the fundamental cloud detection problem for polar night. Liu et al. (2004) compared ground-based radar/lidar data to MODIS cloud mask results using the new polar night spectral tests (included in the cloud mask algorithm for Collection 5) and those from Collection 4 (previous operational version) and found that the misidentification rate of cloud as clear decreased from 44.2% to 16.3% at two Arctic stations. The misidentification of clear as cloud remained at about 8%. In Collection 5 of the MODIS cloud mask, two spectral cloud tests were modified, two were added, and one clear-sky restoral test was added when processing polar night scenes.

## 1) 11–3.9 $\mu\text{m}$ BRIGHTNESS TEMPERATURE DIFFERENCE (BTD) LOW CLOUD TEST

The 11–3.9  $\mu\text{m}$  BTD low cloud test is based on the differential absorption between these two wavelengths by both water and ice cloud particles. The nighttime BTD may be either negative or positive depending on cloud optical depth and particle size (Liu et al., 2004). However, the situation becomes more complex in temperature inversions that are frequent in polar night conditions. For a complete discussion of the problem, see Liu et al. (2004). Previous 11-3.9  $\mu\text{m}$  test thresholds did not take temperature inversions into account and were most appropriate for non-polar, thick water clouds. For Collection 5, the high confident cloud thresholds vary linearly from –0.8 to +0.6 as the 11  $\mu\text{m}$  brightness temperature (BT) varies between 235K and 265K. The threshold is constant below 235K and above 265K. Figure 2b shows an example of test results on April 1, 2003 beginning at 05:05 UTC from northwest Canada. Figure 2a shows imagery of MODIS 11  $\mu\text{m}$  BTs for the same scene. Note that north is at the bottom and west is to the right in these images. In all test result figures, white means cloud indicated, gray means no cloud indicated and black means test not performed.

## 2) 3.9-12 $\mu\text{m}$ BTD HIGH CLOUD TEST

The 3.9-12  $\mu\text{m}$  BTD high cloud test has been modified for polar night conditions. For reasons not well understood, the thresholds for this test need to be increased with decreasing temperatures below 265K. This is counter-intuitive from arguments based on atmospheric water vapor loading and absorption at these two wavelengths. Perhaps the calibration of one or both bands is of reduced accuracy at cold temperatures. In addition, the test cannot be used on the very coldest and driest scenes (surface elevations greater than 2000 m) such as are found in Antarctica and Greenland

during the winter season. Therefore, the test is not performed in polar night conditions when the elevation exceeds 2000 m. The Collection 5 confident cloud threshold varies linearly from +4.5K to +2.5K as the 11  $\mu\text{m}$  BT varies between 235K and 265K. The threshold is constant below 235K and above 265K. Figure 2d shows an example of test results from the same scene as above.

### 3) 11-12 $\mu\text{m}$ BTD THIN CIRRUS TEST

Previous versions of the cloud mask algorithm made use of this test only over surfaces not covered by snow or ice. The Collection 5 test makes use of thresholds taken from Key (2002) who extended the Saunders and Kriebel (1988) values to very low temperatures. The modified test has replaced the original in all processing paths for both day and night processing except for Antarctica. Figure 2c shows example results from the same scene as above. At these very cold scene temperatures, the 11-12  $\mu\text{m}$  BTD starts to become noisy as seen at middle left.

### 4) 7.2-11 $\mu\text{m}$ BTD CLOUD TEST

The most significant change to the polar night algorithm is the addition of a new 7.2-11 $\mu\text{m}$  BTD cloud test. Since the weighting function of the 7.2  $\mu\text{m}$  band peaks at about 800 hPa, the BTD is related to the temperature difference between the 800 hPa layer and the surface, which the 11  $\mu\text{m}$  band is most sensitive to. In the presence of low clouds under polar night conditions with a temperature inversion, radiation from the 11  $\mu\text{m}$  band comes primarily from the relatively warm cloud top, decreasing the 7.2-11  $\mu\text{m}$  BTD compared to the clear-sky value. In conditions of deep polar night, even high clouds may be warmer than the surface and will often be detected with this



test. For middle and high clouds in an atmosphere with no inversion, the BTD is lessened because both the 11  $\mu\text{m}$  and 7.2  $\mu\text{m}$  radiances are emanating from near cloud top with little water vapor attenuation in the 7.2  $\mu\text{m}$  band in the dry polar atmosphere. For a complete discussion of the theory, see Liu (2004). The test as configured in MOD35 is applicable only over nighttime snow and ice surfaces. Because the 7.2  $\mu\text{m}$  band is sensitive to atmospheric water vapor and also because inversion strength tends to increase with decreasing surface temperatures over snow covered land (Liu, 2004), thresholds for this test are a function of the observed 11  $\mu\text{m}$  BT. The thresholds vary linearly in three ranges: BTD +2K to -4.5K for 11  $\mu\text{m}$  between 220K and 245K, BTD -4.5K to -11.5K for 11  $\mu\text{m}$  between 245 and 255K, and BTD -11.5 to -21K for 11  $\mu\text{m}$  between 255K and 265K. Thresholds are constant for 11  $\mu\text{m}$  below 220K or above 265K. The thresholds are slightly different over ice (frozen water surfaces): BTD +2K to -4.5K for 11  $\mu\text{m}$  between 220K and 245K, BTD -4.5K to -17.5K for 11  $\mu\text{m}$  between 245 and 255K, and BTD -17.5 to -21K for 11  $\mu\text{m}$  between 255K and 265K. These somewhat larger BTDs presumably reflect a lesser tendency for strong inversions and higher water vapor loading over frozen water surfaces as opposed to snow-covered land areas. These thresholds also differ slightly from those reported in Liu (2004), a result of extensive testing over many scenes and the necessity of meshing this test with other cloud mask tests and algorithms. Note that this test was also implemented for non-polar (latitude < 60 deg.), nighttime snow-covered land. Figure 2e shows imagery from the 7.2  $\mu\text{m}$  band for this same scene from Canada and Figure 2f shows the results of the test. Note the difference in texture between cloudy and clear on the right in the 7.2  $\mu\text{m}$  BT imagery, even though the gray scale indicates similar temperatures for much of the scene. Clouds indicated on the left are just barely seen in Figure 2a.

## 5) 7.2-11 $\mu\text{m}$ BTD CLEAR SKY TEST

The MODIS cloud mask employs several spectral tests that attempt to identify unambiguously clear pixels in polar night conditions. Positive results override any cloud indications. A 7.2-11  $\mu\text{m}$  BTD test may be utilized to find clear sky because of the prevalence of polar night temperature inversions. This test works in the same way as the current 6.7-11  $\mu\text{m}$  BTD clear-sky restoral test, where 11  $\mu\text{m}$  BTs are sometimes significantly lower than those measured in the 6.7  $\mu\text{m}$  band because the 6.7  $\mu\text{m}$  weighting function peaks near the top of a warmer inversion layer in some cases. However, since the 7.2  $\mu\text{m}$  band peaks lower in the atmosphere, a 7.2-11  $\mu\text{m}$  BTD test can detect lower and weaker inversions. Pixels are restored to clear if the 7.2-11  $\mu\text{m}$  BTD  $> 5\text{K}$ .

### *b. Polar Daytime Snow*

A new version of the 3.9-11  $\mu\text{m}$  test has been developed for polar, daytime conditions. The test thresholds are now dependent on the observed 11  $\mu\text{m}$  BT when that BT is lower than 245K. Also, the test will no longer be performed at all when the 11  $\mu\text{m}$  BT is below 230K. During Arctic and Antarctic spring and autumn seasons, the sun is above the horizon but surface temperatures and hence clear-sky observed BTs are still very low, sometimes  $< 200\text{K}$  at 11  $\mu\text{m}$  on the Antarctic plateau near the South Pole. Under these conditions, and adding just a small amount of solar insolation, the extreme nonlinearity of the Planck function at 3.9  $\mu\text{m}$  makes the 3.9-11  $\mu\text{m}$  BTD higher than one would expect for clear-sky observations at warmer temperatures. This effect, along with the use of static test thresholds was leading to false cloud determinations in Antarctica and Greenland. The new thresholds will vary between 7.0K and 14.5K as 11  $\mu\text{m}$  BTs vary between

245K and 230K at the 0.5 clear-sky confidence level. Above 245K, the threshold will remain as before, at 7K.

#### *c. Arctic Cloud Frequency Comparisons*

Figures 3a-3f show mean Arctic cloud frequencies from Aqua MODIS Collection 5 cloud mask and APP-X (AVHRR Polar Pathfinder-Extended) (Key, 2002) data and differences between them during day and night for the period January 2003 – December 2004. MODIS cloud amounts are generally higher than APP-X during daytime (warm season), especially in N. Canada, Siberia, and Greenland. At night (cold season), differences are generally smaller except for some portions of Greenland's east coast and the Canadian archipelago. Figure 4 shows time series of monthly mean cloud frequencies for the two data sets, day and night separately. Note that from May through September, the daytime values compare very well, then diverge rapidly as polar darkness descends. At night, December through April values are quite similar. The Warren et al. (1986, 1988) values for day and night together are shown (black line) for reference. Distributions of MODIS minus APP-X cloud fractions for day (blue curve) and night (red curve) are shown in Figure 5. Greater uncertainty between the two data sets is expected during nighttime conditions due to less available information delineating clear skies from cloudy. The mode is +5%.

#### *d. Nighttime Land*

The major enhancement to nighttime land processing is the inclusion of a surface temperature (SFCT) test. Gridded surface air temperatures from Global Data Assimilation System (GDAS) model output fields (Derber et al., 1991) are compared to observed 11  $\mu\text{m}$  BTs. Due to large variations of SFCT in mountainous areas and large diurnal swings in desert regions that are not

always well characterized in the gridded data, the test is not performed there. Even with these restrictions, great care must be taken when applying this test. Thresholds of GDAS SFCT minus 11  $\mu\text{m}$  BT are set at 12K for vegetated areas and 20K for semi-arid lands but are adjusted for viewing zenith angle and water vapor loading based on 11-12  $\mu\text{m}$  BTs. The basic thresholds are increased by 2 times the 11-12  $\mu\text{m}$  BT and non-linearly with viewing zenith angle, from 0K at nadir to a maximum of 3K at the edge of scan. With threshold values set this high, the test can obviously function only as a gross cloud test. But it is particularly useful for detecting thick mid-level clouds that are surprisingly difficult to detect at night over land. The test is also performed on snow-free polar scenes.

#### *e. Nighttime Ocean*

Nighttime ocean cloud detection has undergone major changes. A sea-surface temperature (SST) test and an 8.6-7.2  $\mu\text{m}$  BT test have been implemented for the first time. A new 11  $\mu\text{m}$  BT variability test has also been included. The Reynolds SST (Reynolds and Smith, 1994) minus 11  $\mu\text{m}$  BT test has the same function as the land surface temperature test, namely as a gross cloud test. Because of more uniform ocean surface temperatures, the threshold can be lowered to a base value of 6K that is adjusted to account for viewing zenith angle and water vapor loading in the same way as described above for the land case.

An 8.6-7.2  $\mu\text{m}$  BT test has been added and is designed primarily to detect thick mid-level clouds but can also detect lower clouds in regions of low relative humidity in the middle atmosphere. It is sometimes more effective than the SST test for finding stratocumulus clouds of small horizontal extent. It can also detect high, thick clouds. Both this and the SST test are needed

in order to find those clouds that are thick but that also show very small thermal spatial variability. The test thresholds are 16.0K, 17.0K, and 18.0K for 0.0, 0.5, and 1.0 confidence of clear sky, respectively.

The 11  $\mu\text{m}$  variability test has been modified to detect clouds of small spatial extent (a pixel or two) and cloud edges. Most thick clouds are now found by other tests but a variability test is very effective at night for detecting the thinner, warmer cloud edges over the uniform ocean surface. The previous (Collection 4) test determined a standard deviation over the pixel of interest and the eight surrounding. Then, a very stringent threshold was used to determine cloudiness. In the Collection 5 version, the number of differences  $\leq 0.5\text{K}$  in 11  $\mu\text{m}$  BT between each surrounding pixel and the center one are counted. The higher the number (8 possible), the more likely the center pixel is clear. The confident cloud and confident clear thresholds are 3 and 7, respectively. Figures 6a-6d show example results from the above tests for an ocean scene with widespread stratus clouds in the subtropical southern Pacific west of South America.

The quality of the MODIS nighttime ocean cloud mask algorithm has seen a major improvement. The changes noted above have lowered the retrieved cloud amounts to reasonable levels and compare favorably with daytime values. This is a result of better detection of above-freezing clouds and use of less stringent BT variability thresholds. Figure 7a shows zonal mean values of nighttime ocean clear-sky frequencies for one day from Terra Collection 4 and 5 algorithms. Though the locations of minima and maxima stay the same, clear sky amounts increase by as much as 10% over the southern ocean and by as much as 20% over the northern subtropics.

To further investigate the quality and consistency of the nighttime ocean cloud mask, sea surface temperatures (SSTs) were computed and analyzed for the eastern Pacific (-45 to +45

latitude and 180 to 130 west longitude) over an eight-day period from April 1-8, 2003. Single-pixel values from day and night were calculated separately, then binned into 0.25K histogram classes and compared with each other, as well as to the Reynolds SST data from the same locations and times. The current MODIS SST equation and coefficients (Brown et al, 1999) were used (but not the entire algorithm) along with clear-sky 11  $\mu\text{m}$  BTs and 11-12  $\mu\text{m}$  BTDs, where clear-sky was determined solely from the C5 MODIS cloud mask (probably clear and confident clear designations). No 4  $\mu\text{m}$  data was used at night and no pre-processing or post-processing screening was performed except to eliminate obviously bad radiance data. The purpose of this exercise was not to produce the best SST possible, but rather to show that the ocean cloud mask performs well and is reasonably consistent between day and night. Figure 7b shows a histogram of SST values obtained for day and night in 0.25K classes. The difference in the peak class between day and night is 0.25K. Figure 7c shows a histogram with the same class widths but where the MODIS SSTs were compared to those of the Reynolds data set. The Reynolds values did not change from day to night. The peak in the difference (MODIS – Reynolds) distribution lies at  $-0.25\text{K}$  for both day and night, though there are less nighttime values for all difference classes warmer than the peak value and more for all less than the peak. This is undoubtedly mostly due to a little more cloud contamination in the nighttime clear-sky BTs, though direct observations of SST show a diurnal cycle of up to a degree or so in some situations (Webster et al., 1995). Nevertheless, 82.1% of daytime and 68.6% of nighttime MODIS SSTs are within 1 degree of the Reynolds values on average, using nothing but MOD35 to determine the input BTs. Figure 7d shows the zonal mean daytime MODIS SSTs and day minus night differences. The fit to the differences is a 5<sup>th</sup>-order polynomial. The larger zonal mean differences are seen in higher latitudes to both north and south where more clouds are present and

SSTs are lower. This is an indication that cloud edges are not as effectively screened out by the nighttime algorithm. From Figure 9b one can see that, for the MOD35 algorithm, about 10% of ocean cloudy pixels are detectable only by use of visible and NIR data.

Another exercise has compared SSTs generated from MODIS (MOD28) with those from AMSR-E (Advanced Microwave Scanning Radiometer for the Earth Observing System) and TMI (Tropical Rainfall Measuring Mission Microwave Imager), but where differences are reported as functions of the MOD35 cloud categories. Global data, including sun-glint and nighttime observations from December 13, 2006 were used. Figure 8 shows MODIS SSTs minus MWSSTs (microwave SSTs from AMSR-E and TMI) as functions of clear-sky confidence. Modal values of the differences in confident clear cases are -0.1K for both day and night. Error values listed are percents of values  $< -2K$  minus percents  $> +2K$  for confident clear, probably clear and probably cloudy. For confident cloud, error value is percent between -2K and +2 K. As in Fig. 7, these histograms indicate that MOD35 is an effective cloud detection method during both day and night, but also that the four cloud mask output categories may be used as a kind of “quality flag” for derived products that rely heavily on unobstructed views of the surface.

#### *f. Sun-glint and Daytime Ocean*

Improvements have been made to the cloud mask in sun-glint regions and in daytime oceans generally. The SST test has been implemented in the daytime ocean algorithm exactly as in the nighttime case. For areas not affected by sun-glint, the improvements are small since the algorithm has already been well developed for some time. The most noticeable change is more confident cloud and less uncertain for scenes containing thin cirrus. The changes are more dramatic for areas

affected by sun-glint. Many low-level clouds with above-freezing cloud top temperatures have been moved from the uncertain to the confident cloud category by use of the SST test. Much of the ambiguity between bright clouds and sometimes equally bright ocean surfaces on the one hand, and between warm clouds and warm ocean surfaces on the other, is ameliorated by knowledge of the SST.

In addition, a new clear-sky restoral test is applied. When no thermal tests indicate the presence of cloud, the mean and standard deviation of 0.86  $\mu\text{m}$  reflectances are computed over the pixel of interest and the eight surrounding. Pixels are declared to be probably clear (confidence 0.96) when the standard deviation multiplied by the mean is  $< 0.001$ . This has the effect of restoring to clear many pixels that are bright in the visible and NIR but also very uniform. This test is performed in addition to previously existing restoral tests.

To demonstrate the improvements in the cloud mask sun-glint algorithm and the consistency of results between sun-glint and non sun-glint pixels, a region of the Pacific Ocean between  $-30$  and  $+45$  latitude was chosen for a detailed study. The longitudinal domain was  $-180$  to  $-130$  and the temporal range was April 1-8, 2003. Figure 9a shows total cloud amount as a function of glint angle binned in 6-degree increments. Sun-glint is defined in the cloud mask algorithm as glint angles from 0 to 36 degrees, where 0 defines the specular point (Ackerman et al, 1998). Because increasing sun-glint angles on the Earth's surface are characterized by a series of concentric circles, larger glint angles also imply a wider range of latitudes, as well as increasing surface area and viewing zenith angles.

At first glance, the total cloud amount from the combined confident cloudy and uncertain decisions from MOD35 (top curve) would appear to be seriously biased in the sun-glint regions, but



other indications of cloud (bottom curves) show the same pattern. Sub-freezing observations in the 11  $\mu\text{m}$  band are independent of sun-glint, and thin and thick cirrus as determined by 1.38  $\mu\text{m}$  reflectances, are generally insensitive to glint in moist, tropical regions. In addition, a L1b cross-talk calibration correction to this band removes most, if not all, of the sun-glint signal that might interfere with cloud detection in the dryer subtropical areas characterized by atmospheric subsidence. The numbers in brackets along the top curve indicate the minimum and maximum latitudes from which the corresponding values originated.

Figure 9b shows total cloud frequency from the same region but from non-glint pixels and as a function of latitude. It can be seen from comparing the latitude ranges from the first plot to the cloud frequencies of those latitudes on the second, that the trend toward lower cloud amounts in the latitudes most affected by glint is reasonable. Using the total number of observations from each glint angle bin as a surrogate for areal coverage (not exact), a reasonably accurate weighted average may be obtained over the entire region. The non-glint cloud amount was 70.8% while the cloud percentage from the glint region was 64.5%, a difference of 6.3%. Although not proven by this analysis, we suspect that the majority of missed cloudy pixels in glint areas are those warm clouds of small extent that would otherwise be detected exclusively by visible and NIR cloud tests. In areas affected by glint, the background ocean reflectance is often about the same or greater than that from these clouds, rendering them invisible. The bottom curve on Figure 9b shows zonal means of the frequencies of these clouds as defined by the cloud mask from non-glint regions.

### **3. Conclusions**

Changes for Collection 5 reprocessing in the MODIS cloud mask are described in this paper. They include changes in the polar night, ocean and land night, polar day snow, and sun-glint

processing paths. Including tests for thin cirrus clouds (11-12  $\mu\text{m}$  and 7.2-11  $\mu\text{m}$  BTDs) will enhance the cloud detection capability in polar night conditions, while a new clear-sky restoral test (also 7.2-11  $\mu\text{m}$  BTD) will allow more surface temperature inversions to be located that are normally cloud-free. Users of the cloud mask will see an increase in the number of pixels flagged as cloudy under polar night conditions. The nighttime ocean algorithm has been reworked so that a more realistic amount of clouds are detected. Night ocean cloud amounts now compare well with those from daytime data. An analysis of SST using only MOD35 for cloud screening shows that a product that is very sensitive to small amounts of cloud contamination generates reasonable results from both the day and night algorithms. It is not apparent that the nighttime SSTs shows more cloud contamination than the daytime ones above that which may be expected due to lack of visible and NIR data. Zonal mean SST differences between day and night range from 0.25K in the warmest regions to about 1K in colder, cloudier areas. Day and night distributions of Reynolds SSTs vs. SSTs using MOD35 peak at  $-0.25\text{K}$ , with the Reynolds SST being warmer. A study of cloud amount as a function of sun-glint angle reveals that the cloud mask does a reasonable job in the difficult glint regions. An 8-day, area-weighted average of cloud amounts between glint and non-glint areas shows a deficit of 6.3% from glint regions. We suspect this difference is due to warm clouds of small areal extent that cannot be reliably detected by IR tests and that fade into the visible and NIR glint background reflectances. Users will see a marked decrease in false cloud determinations in daylight conditions during the spring and fall seasons in Greenland and Antarctica. This is due to a modification in the 3.9-11  $\mu\text{m}$  BTD test.

## **Acknowledgements**

The authors would like to graciously thank the MODIS science team, in particular: P. Menzel, A. Heidinger, C. Moeller, B. Baum, C. Schaaf, M. King, V. Salmonson and S. Platnick for their help in the development and testing of the MODIS cloud mask. This research was funded under NASA grants NNG04HZ38C and NNG04GL14G; NNG04GB93G also contributed to this study. NOAA/NESDIS requires the following: "The views, opinions, and findings contained in this report are those of the author(s) and should not be construed as an official National Oceanic and Atmospheric Administration or U.S. Government position, policy, or decision." The authors continue to appreciate the support provided by the MODIS Characterization and Support Team and the MODIS Science Data Support Team. These research efforts have been supported by a number of agencies and research programs; a particular acknowledgement is due the NASA Radiation Sciences Program and the NASA Earth Observing System Project Science Office.

## Appendix: Cloud Mask Test Thresholds

Tables 1-3 list the IR and visible/NIR cloud test thresholds, and the clear-sky restoral test thresholds, respectively, used in the MODIS cloud mask. Values are the same for both Terra and Aqua instruments unless indicated. Abbreviations are listed after Table 3.

Individual cloud test thresholds have been developed in accordance with radiative transfer theory but “fine-tuned” for specific surface and cloud types, and in some cases different instruments (Aqua, Terra). They are also calculated to be “clear-sky conservative”. For the MODIS cloud mask, this means that each cloud test detects as many cloudy pixels as possible without generating unacceptable numbers of false positives in the final result. The final values are derived after testing many scenes in various seasons and under changing viewing geometries. Testing is also performed after any changes to the radiometric calibration of bands used in the cloud mask. In this sense, the tuned thresholds are empirical in nature.

Clear-sky restoral tests may override the computed confidence of clear sky in some cases. These are applied only after all cloud tests have been applied and combined to form a clear-sky confidence (Eq. 1, 2 in the main text). The need for these underscores the difficulty of *global* cloud detection, where pixel-by-pixel, regional and global, and temporal cloud statistics are required at high accuracy. There are three situations that are particularly problematic for global cloud detection algorithms: sun-glint, unobstructed land surfaces that are as reflective as some clouds, and polar night conditions where little thermal contrast is present between surfaces and clouds. In the polar case, we look for evidence of deep atmospheric temperature inversions that indicate clouds are very unlikely. In sun-glint and bright land situations, unambiguous measures of clear sky are more difficult to define, but we use a combination of visible/NIR and IR tests that increase the confidence of clear sky when appropriate.

Table 1. IR cloud test thresholds used in the MODIS cloud mask (MOD35) and the scene types for which the tests are applied.

MODIS IR Cloud Test Thresholds (MOD35)		
IR Test	Thresholds for Confidence Limits (0.0, 0.5, 1.0 or low, middle, high)	Scenes
11 $\mu\text{m}$ ("freezing" test)	267K, 270K, 273K	all ocean
13.9 $\mu\text{m}$	222K, 224K, 226K	all non-polar
6.7 $\mu\text{m}$	215K, 220K, 225K	all except Antarctic night
sfc. temp. - 11 $\mu\text{m}$	6K modified by VZA and 11-12 $\mu\text{m}$ BTD +1K/-2K lo/hi	Day, night deep ocean
sfc. temp. - 11 $\mu\text{m}$	same as above but base threshold = 10K	day, night shallow ocean
sfc. temp. - 11 $\mu\text{m}$	12K modified by VZA and 11-12 $\mu\text{m}$ BTD +/- 2K lo/hi	non-arid night land
sfc. temp. - 11 $\mu\text{m}$	20K modified by VZA and 11-12 $\mu\text{m}$ BTD +/- 2K lo/hi	arid, semi-arid night land
11-12 $\mu\text{m}$ BTD	Function of VZA and 11 $\mu\text{m}$ BT (Key, 2002) confidence limits vary by scene type, latitude	all except Antarctica
11, 12, 8.6 $\mu\text{m}$ (tri-spectral test)	8.6-11 $\mu\text{m}$ BTD threshold based on 11-12 $\mu\text{m}$ BT, +/- 0.5K lo/hi	all ocean
11-3.9 $\mu\text{m}$ BT	-14K, -12K, -10K	non-arid day land
11-3.9 $\mu\text{m}$ BT	-20K, -18K, -16K	arid, semi-arid day land 11 $\mu\text{m}$ BT $\leq$ 320K
11-3.9 $\mu\text{m}$ BT	10K, 7K, 4K	day snow/ice

	14K, 10K, 6K for elevations > 2000 m	
11-3.9 $\mu\text{m}$ BT	11-12 $\mu\text{m}$ BT > +1.00: -2.0K, -2.5K, -3.0K 11-12 $\mu\text{m}$ BT < -1.00: +5.0K, +4.5K, +4.0K -1 $\leq$ 11-12 $\mu\text{m}$ BT $\leq$ +1: LI between -2.5K and +4.5K, +/- 0.5K lo/hi	night land
11-3.9 $\mu\text{m}$ BT	0.7K, 0.6K, 0.5K	night snow/ice
11-3.9 $\mu\text{m}$ BT	-10K, -8K, -6K	day ocean
11-3.9 $\mu\text{m}$ BT	1.25K, 1.00K, -1.00K	night ocean
11-3.9 $\mu\text{m}$ BT	11 $\mu\text{m}$ BT < 235K: -0.1K, -0.2K, -0.3K 11 $\mu\text{m}$ BT > 265K: +1.1K, +1.0K, +0.0K 235K $\leq$ 11 $\mu\text{m}$ BT $\leq$ 265K: LI between -0.2K and +1.0K, +/- 0.1K lo/hi	polar night land, snow/ice
11-3.9 $\mu\text{m}$ BT	11 $\mu\text{m}$ BT < 230K: -17.5K, -14.5K, -11.5K 11 $\mu\text{m}$ BT > 245K: -10K, -7K, -4K 230K $\leq$ 11 $\mu\text{m}$ BT $\leq$ 245K: LI between -14.5K and -7K, +/- 3K lo/hi	polar day snow/ice 11 $\mu\text{m}$ BT > 230K
3.9-12 $\mu\text{m}$ BT	15K, 10K, 5K	Night land
3.9-12 $\mu\text{m}$ BT	4.5K, 4.0K, 3.5K	night snow
3.9-12 $\mu\text{m}$ BT	11 $\mu\text{m}$ BT < 235K: 4.5K, 4.0K, 3.5K 11 $\mu\text{m}$ BT > 265K: 2.5K, 2.0K, 1.5K 235 $\leq$ 11 $\mu\text{m}$ BT $\leq$ 265K: LI between 4.0K and 2.0K, +/- 0.5K lo/hi	polar night snow/ice (elevation $\leq$ 2000 m)
7.2-11 $\mu\text{m}$ BT	-8K, -10K, -11K	Night land, 11-3.9 $\mu\text{m}$ $\leq$ -2K

7.2-11 $\mu\text{m}$ BTD	<p>11 <math>\mu\text{m}</math> BT &lt; 220K: -1K, 0K, 1K</p> <p>220K &lt; 11 <math>\mu\text{m}</math> BT &lt; 245K: LI between 0K and -4.5K, -/+ 1K lo/hi</p> <p>245K <math>\leq</math> 11 <math>\mu\text{m}</math> BT &lt; 255K: LI between -4.5K and -10.5K, -/+ 1K lo/hi</p> <p>255K <math>\leq</math> 11 <math>\mu\text{m}</math> BT <math>\leq</math> 265K: LI between -10.5K and -20K, -/+ 1K lo/hi</p> <p>11 <math>\mu\text{m}</math> BT &gt; 265K: -21K, -20K, -19K</p>	polar night land, night snow
7.2-11 $\mu\text{m}$ BTD	<p>11 <math>\mu\text{m}</math> BT &lt; 220K: 0K, 1K, 2K</p> <p>220K <math>\leq</math> 11 <math>\mu\text{m}</math> BT &lt; 245K: LI between 1K and -7K, -/+ 1K lo/hi</p> <p>245K <math>\leq</math> 11 <math>\mu\text{m}</math> BT &lt; 255K: LI between -7K and -16.5K, -/+ 1K lo/hi</p> <p>255K <math>\leq</math> 11 <math>\mu\text{m}</math> BT <math>\leq</math> 265K: LI between -16.5K and -20K, -/+ 1K lo/hi</p> <p>11 <math>\mu\text{m}</math> BT &gt; 265K: -21K, -20K, -19K</p>	night ice
8.6-7.2 $\mu\text{m}$ BTD	16K, 17K, 18K	night ocean 11 $\mu\text{m}$ BT $\geq$ 280K for polar night ocean
11 $\mu\text{m}$ BT variability number surrounding pixel BTs minus center pixel BT $\leq$ 0.5K	3, 6, 7	night ocean

Table 2. Visible and NIR cloud test thresholds used in the MODIS cloud mask (MOD35) and the scene types for which the tests are applied.

MODIS VIS/NIR Cloud Test Thresholds (MOD35)		
VIS/NIR Test	Thresholds for Confidence Limits (0.0, 0.5, 1.0 or low, middle, high)	Scenes
0.86 $\mu\text{m}$ REF	Aqua 0.065, 0.045, 0.030 Terra 0.055, 0.040, 0.030	non-glint unfrozen day ocean
0.86 $\mu\text{m}$ REF	0.34, 0.30, 0.26	arid, semi-arid day land (no snow)
0.86 $\mu\text{m}$ REF	glint angle 0-10°: 0.115, 0.105, 0.095 glint angle 10-20°: LI between 0.105 and 0.075, +/- 0.01 lo/hi glint angle 20-36°: LI between 0.075 and 0.045, +/- 0.01 lo/hi (Aqua) LI between 0.075 and 0.040, +/- 0.01 lo/hi (Terra)	Sun-glint
0.66 $\mu\text{m}$ REF	0.22, 0.18, 0.14	non-snow, non-arid day land
1.38 $\mu\text{m}$ REF	0.040, 0.035, 0.030	day scenes except snow/ice elevation $\leq$ 2000 m
1.38 $\mu\text{m}$ REF	0.0600, 0.0525, 0.0450	day snow/ice elevation $\leq$ 2000 m
0.86/0.66 $\mu\text{m}$ REF ratio	0.95, 0.90, 0.85	non-glint unfrozen day ocean
0.86/0.66 $\mu\text{m}$ REF ratio	1.05, 1.00, 0.095	Sun-glint
0.86/0.66 REF ratio (modified GEMI)	1.85, 1.90, 1.95	non-coastal, non-arid day land (no snow)



Table 3. Clear-sky restoral test thresholds used in the MODIS cloud mask (MOD35) and the scene types for which they are applied.

MODIS Clear-sky Restoral Test Thresholds (MOD35)		
Test	Threshold	Scenes
11 $\mu\text{m}$ BT	Aqua: > 295.0K, > 300.0K, > 305.0K Terra: > 292.5K, > 297.5K, > 302.5K assign prob. cloudy, prob. clear, clear (thresholds adjusted for elevation)	day land, no snow, orig. conf. $\leq 0.95$ no IR cloud tests positive
11 $\mu\text{m}$ BT	Aqua: > 290.0K, > 295.0K, > 305.0K Terra: > 287.5K, > 292.5K, > 302.5K assign prob. cloudy, prob. clear, clear (thresholds adjusted for elevation)	non-vegetated land, no snow, orig. conf. $\leq 0.95$ , no IR cloud tests positive
0.55/1.24 $\mu\text{m}$ 3.7-3.9 $\mu\text{m}$ BTD, 3.9-11 $\mu\text{m}$ BTD	0.55/1.24 $\mu\text{m}$ > 3.0 and 3.7-3.9 $\mu\text{m}$ BTD < 11K and 3.9-11 $\mu\text{m}$ BTD < 15K, assign prob. clear	day land, no snow, orig. conf. $\leq 0.95$ , no IR cloud tests positive, above CSR tests negative
11 $\mu\text{m}$ BT	> 287.5K, > 292.5K, > 297.5K assign prob. cloudy, prob. clear, clear (thresholds adjusted for elevation)	non-polar night land, no snow, orig. conf. $\leq 0.95$ no high or middle cloud tests positive
NDVI	NDVI $\leq -0.18$ or NDVI $\geq 0.40$ assign clear	coast and shallow water no high or middle cloud tests positive
3.7-11 $\mu\text{m}$ BTD	$\geq 13\text{K}$ , assign prob. cloudy	sun-glnt, orig. conf. < 0.95, no high, middle, or sfc. temp. cloud tests positive
0.895/0.935 $\mu\text{m}$	> 3.0, assign prob. clear	same as above, positive 3.7-11 $\mu\text{m}$ BTD test

0.86 $\mu\text{m}$ REF	$\sigma$ * mean < 0.001 over 3x3 pixel region, assign prob. clear	same as above, positive 3.7-11 $\mu\text{m}$ BTD test
11 $\mu\text{m}$ BT	8 surrounding pixel BTs minus center pixel BT $\leq 0.5\text{K}$ , assign prob. clear	ocean, $0.66 < \text{orig. conf.} \leq 0.95$
11 $\mu\text{m}$ BT	8 surrounding pixel BTs minus center pixel BT $\leq 0.5\text{K}$ , assign prob. cloudy	ocean, $0.05 < \text{orig. conf.} \leq 0.66$
6.7-11 $\mu\text{m}$ BTD	$> +10\text{K}$ , assign clear	night snow
13.3-11 $\mu\text{m}$ BTD	$> +3\text{K}$ , assign clear	polar night snow
7.2-11 $\mu\text{m}$ BTD	$> +5\text{K}$ , assign clear	polar night snow

LI = linear interpolation, VZA = viewing zenith angle, BT = brightness temperature, REF = reflectance, BTD = brightness temperature difference, NDVI = Normalized Difference Vegetation Index, GEMI = Global Environment Monitoring Index, CSR = clear-sky restoral, lo/hi = low/high confidence of clear sky thresholds for cloud tests, sfc. temp. = surface temperature from ancillary data, orig. conf. = computed confidence of clear sky after all cloud tests performed

## References

- Ackerman, S. A., K. I. Strabala, W. P. Menzel, R. A. Frey, C. C. Moeller, L. E. Gumley, B. A. Baum, S. W. Seemann and H. Zhang, 2006: Discriminating clear-sky from cloud with MODIS algorithm theoretical basis document (MOD35). MODIS Atmosphere web site, 129 pp.
- Ackerman, S. A., K. I. Strabala, W. P. Menzel, R. A. Frey, C. C. Moeller, and L. E. Gumley, 1998: Discriminating clear-sky from clouds with MODIS. *J. Geophys. Res.*, **103(D24)**, 32,141–32,157.
- Brown, O., P. Minnett, R. Evans, E. Kearns, K. Kilpatrick, A. Kumar, R. Sikorski, and A. Závody, 1999: Algorithm theoretical basis document. EOS ATBD web site, 98 pp.
- Derber, J., D. Parrish, and S. Lord, 1991: The new global operational analysis system at the National Meteorological Center. *Weather and Forecasting*, **6**, 538-547.
- Key, J. R., 2002: *The cloud and surface parameter retrieval (CASPR) system for polar AVHRR*. University of Wisconsin, Madison, WI, 36 pp.
- King, M. D., W. P. Menzel, Y. J. Kaufman, D. Tanre', B. C. Gao, S. Platnick, S. A. Ackerman, L. A. Remer, R. Pincus, and P. A. Hubanks, 2003: Cloud and aerosol properties, precipitable water, and profiles of temperature and humidity from MODIS. *IEEE Trans. Geosci. Remote Sens.*, **41**, 442– 458.
- Liu, Y., J. Key, R. Frey, S. Ackerman, and W. Menzel, 2004: Nighttime polar cloud detection with MODIS. *Remote Sens. Env.*, **92**, 181-194.
- Platnick, S., M. D. King, S. A. Ackerman, W. P. Menzel, B. A. Baum, J. C. Rie'di, and R. A. Frey, 2003: The MODIS cloud products: algorithms and examples from Terra. *IEEE Trans. Geosci. Remote Sens.*, **41**, 459– 473.

Reynolds, R., and T. Smith, 1994: Improved global sea surface temperature analyses. *J. Climate*, **7**, 929-948.

Saunders, R., and K. Kriebel, 1988: An improved method for detecting clear sky and cloudy radiances from AVHRR data. *Int. J. of Remote Sens.*, **9**, 123-150.

Warren, S. G., C. J. Hahn, J. London, R. M. Chervin, and R. L. Jenne, 1988: Global distribution of total cloud cover and cloud type amounts over ocean. NCAR Tech. Note NCAR/TN 317+STR, 42 pp. + 170 maps.

Warren, S. G., C. J. Hahn, J. London, R. M. Chervin, and R. L. Jenne, 1986: Global distribution of total cloud cover and cloud type amounts over land. NCAR Tech. Note NCAR/TN 273+STR, 21 pp. + 199 maps.

Webster, P., C. Clayson, and J. Curry, 1995: Clouds, radiation, and the diurnal cycle of sea surface temperature in the tropical western Pacific. Proceedings of the Fifth Atmospheric Radiation Measurement (ARM) Science Team Meeting, *ARM Science Team Meeting* web site.

## Figure Captions

Figure 1. Histogram of 11  $\mu\text{m}$  BTs over frozen ocean from January 1, 2003 near the North Pole.

Figure 2. a) MODIS 11  $\mu\text{m}$  BT image, b) 11-3.9  $\mu\text{m}$  BTD test, c) 11-12  $\mu\text{m}$  BTD test, and d) 3.9-12  $\mu\text{m}$  BTD test. Scene is from 05:05 UTC April 1, 2003.

Figure 2. e) MODIS 7.2  $\mu\text{m}$  BT image, f) 7.2-11  $\mu\text{m}$  test, and g) final mask where white indicates cloudy and probably cloudy categories.

Figure 3. Mean cloud frequency during January 2003 – December 2004 for Aqua MODIS (a,d), APP-x (b,e), and MODIS minus APP-x (c,f) during daytime (left) and nighttime (right).

Figure 4. Time series of Aqua MODIS and APP-x Arctic cloud frequencies for day and night conditions from January 2003 through December 2004 (see legend). Warren et al. overall data from 1951-1986 are shown for reference.

Figure 5. Distributions of cloud frequency differences between Aqua MODIS and APP-x Arctic cloud frequencies for day and night conditions. Time period is January 2003 through December 2004.

Figure 6. Example scene of a) MODIS 3.9  $\mu\text{m}$  BT image, b) SST test, c) MODIS 8.6-7.2  $\mu\text{m}$  BTD test, and d) 11  $\mu\text{m}$  variability test. Data is from 6 April, 2004 at 19:10 UTC.

Figure 7. a) zonal mean nighttime ocean clear sky frequency from MODIS Collections 4 and 5 for April 4, 2003, b) histogram of day and night SSTs using the same SST algorithm and coefficients, c) histogram of MODIS vs. Reynolds SSTs for day and night, and d) zonal mean daytime SSTs and zonal mean day minus night SSTs. SST analysis uses data from the eastern Pacific Ocean (-45 to +45 latitude and -180 to -130 longitude).

Figure 8. Histograms of MODIS minus MWSST SSTs as functions of MOD35 clear sky confidence levels. Daytime data at top, nighttime at bottom.

Figure 9 a) cloud frequencies as a function of sun-glint angle, and b) latitude. The cloud frequencies in (b) do not contain any observations from sun-glint conditions. Data is from April 8, 2003.

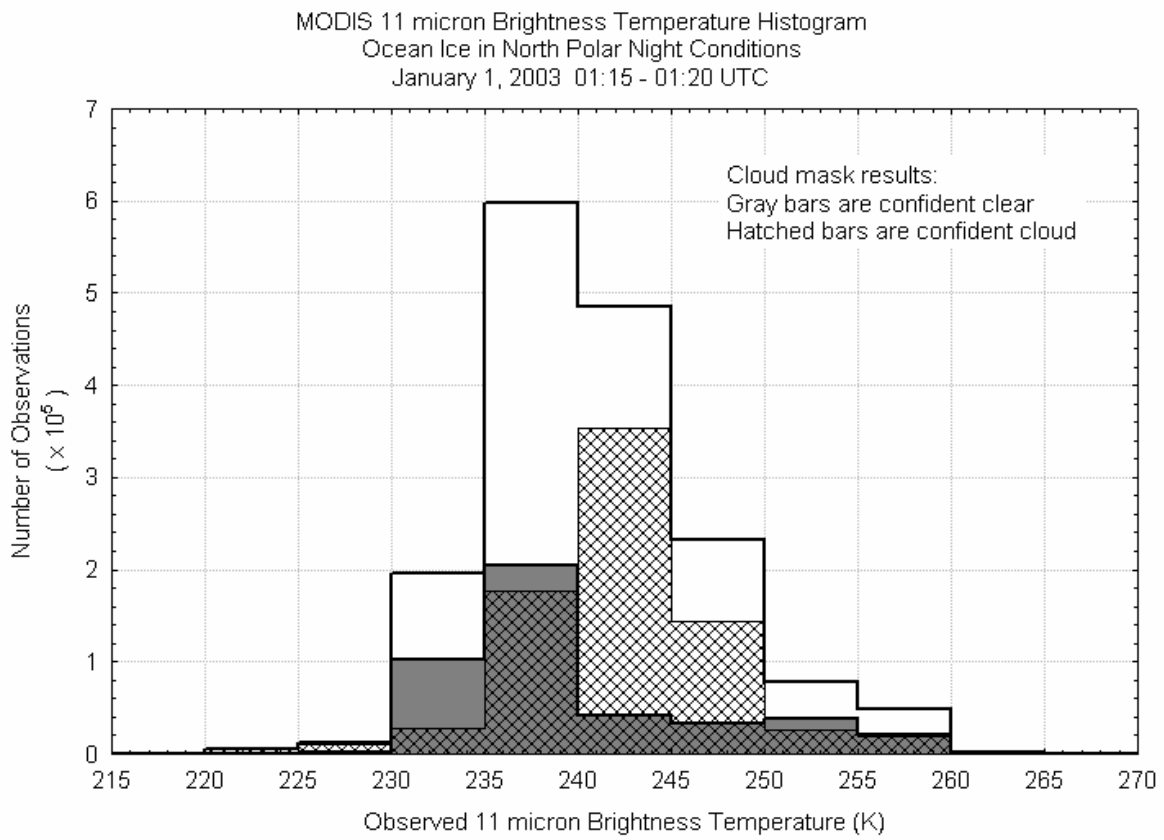


Figure 1. Histogram of 11  $\mu\text{m}$  BTs over frozen ocean from January 1, 2003 near the North Pole.

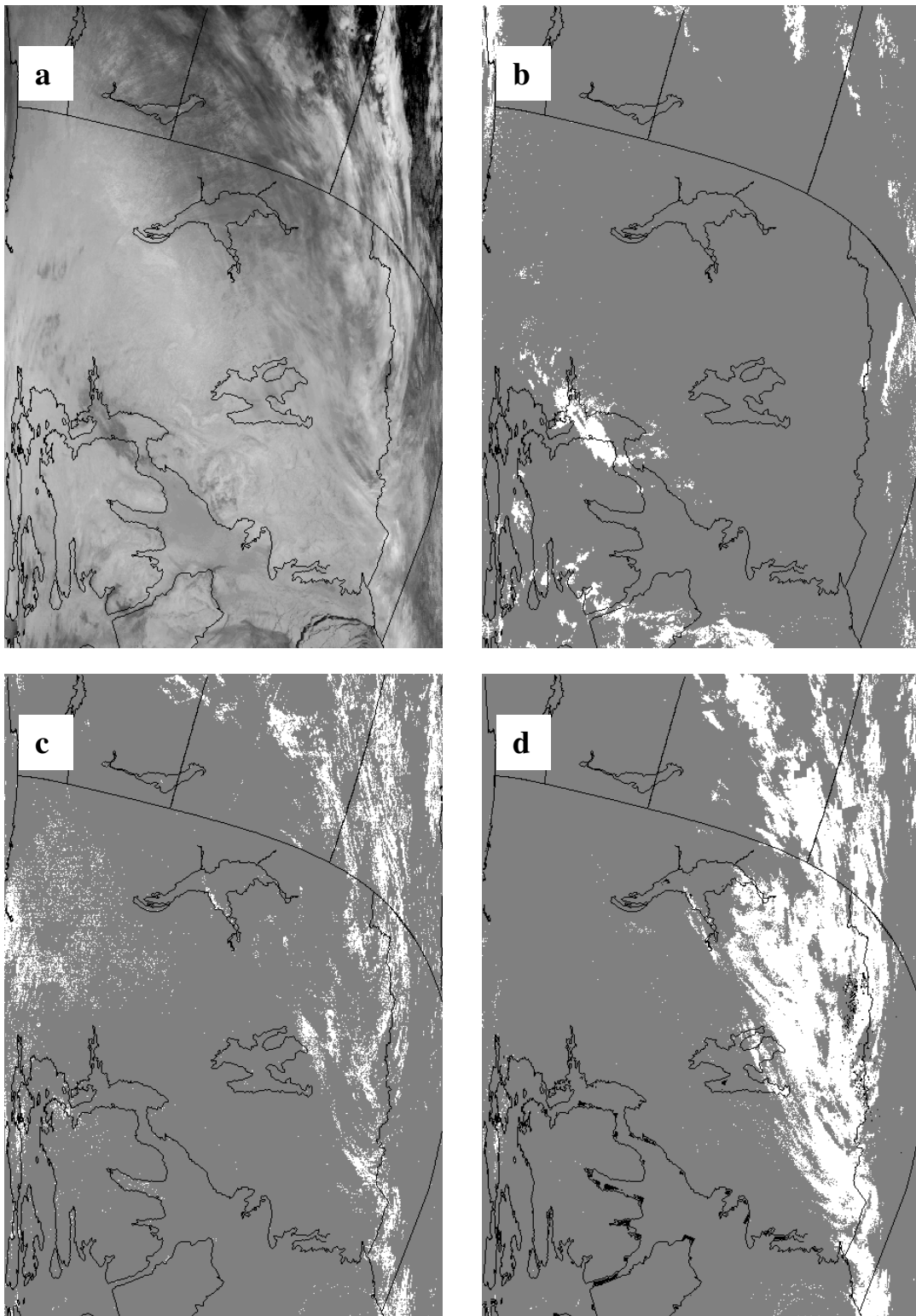


Figure 2. a) MODIS 11  $\mu\text{m}$  BT image, b) 11-3.9  $\mu\text{m}$  BTD test, c) 11-12  $\mu\text{m}$  BTD test, and d) 3.9-12  $\mu\text{m}$  test. Scene is from 05:05 UTC April 1, 2003.



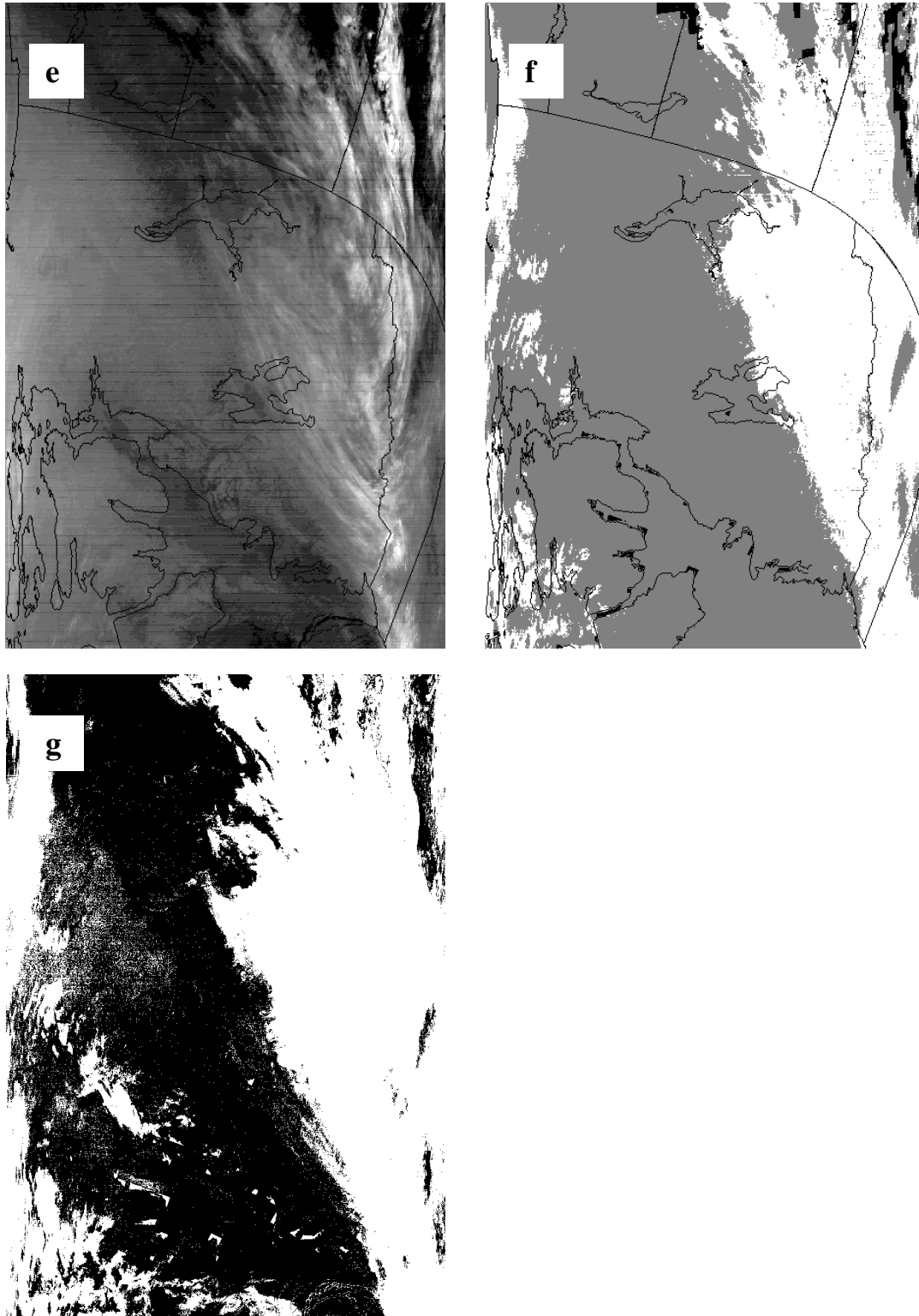


Figure 2. e) MODIS 7.2  $\mu\text{m}$  BT image, f) 7.2-11  $\mu\text{m}$  test, and g) final mask where white indicates cloudy and probably cloudy categories.

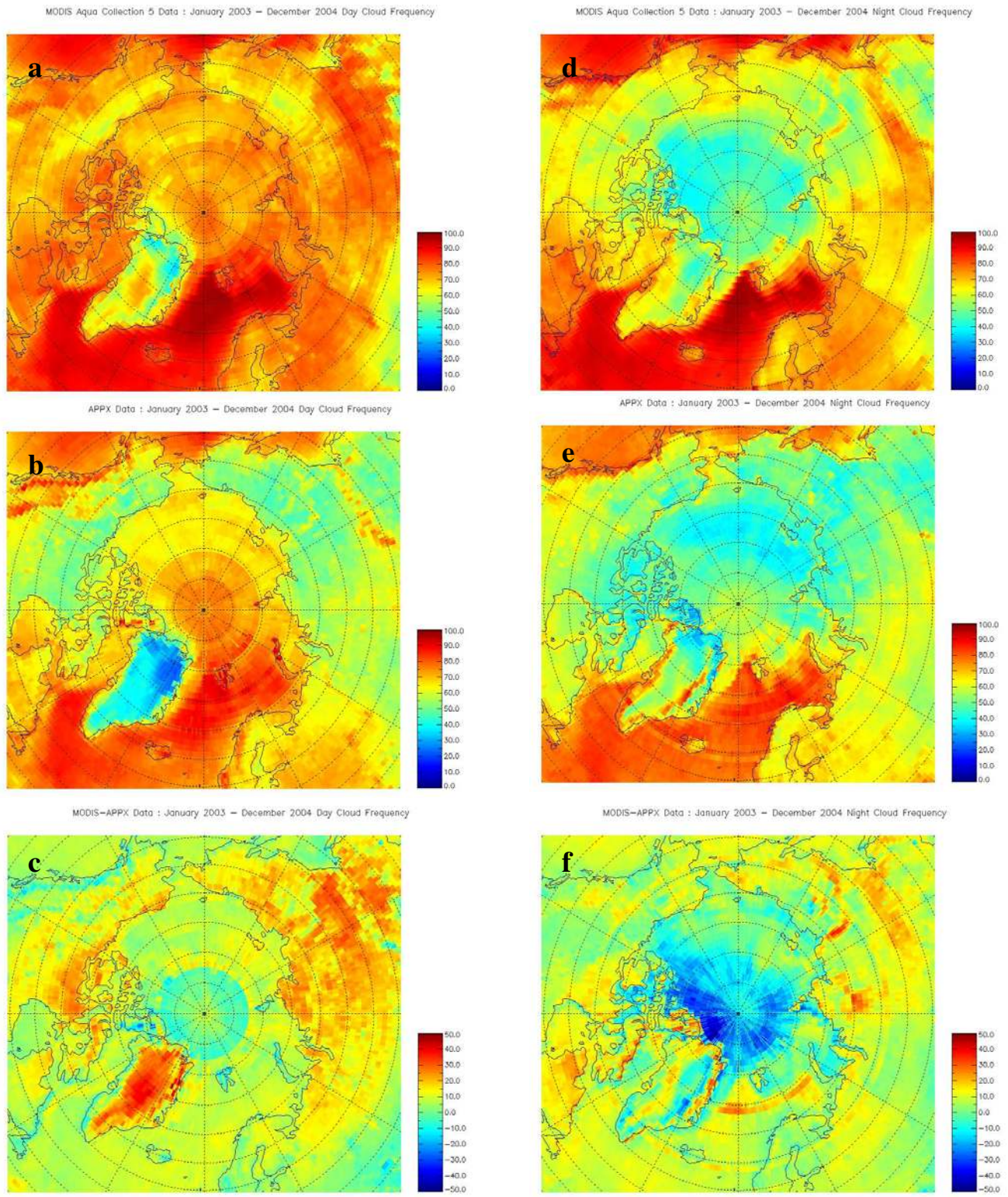


Figure 3. Mean cloud frequency during January 2003 – December 2004 for Aqua MODIS (a,d), APP-x (b,e), and MODIS minus APP-x (c,f) during daytime (left) and nighttime (right).

MODIS and APP-X Arctic Cloud Fraction  
 January 2003 - December 2004  
 Latitude 62-90 North

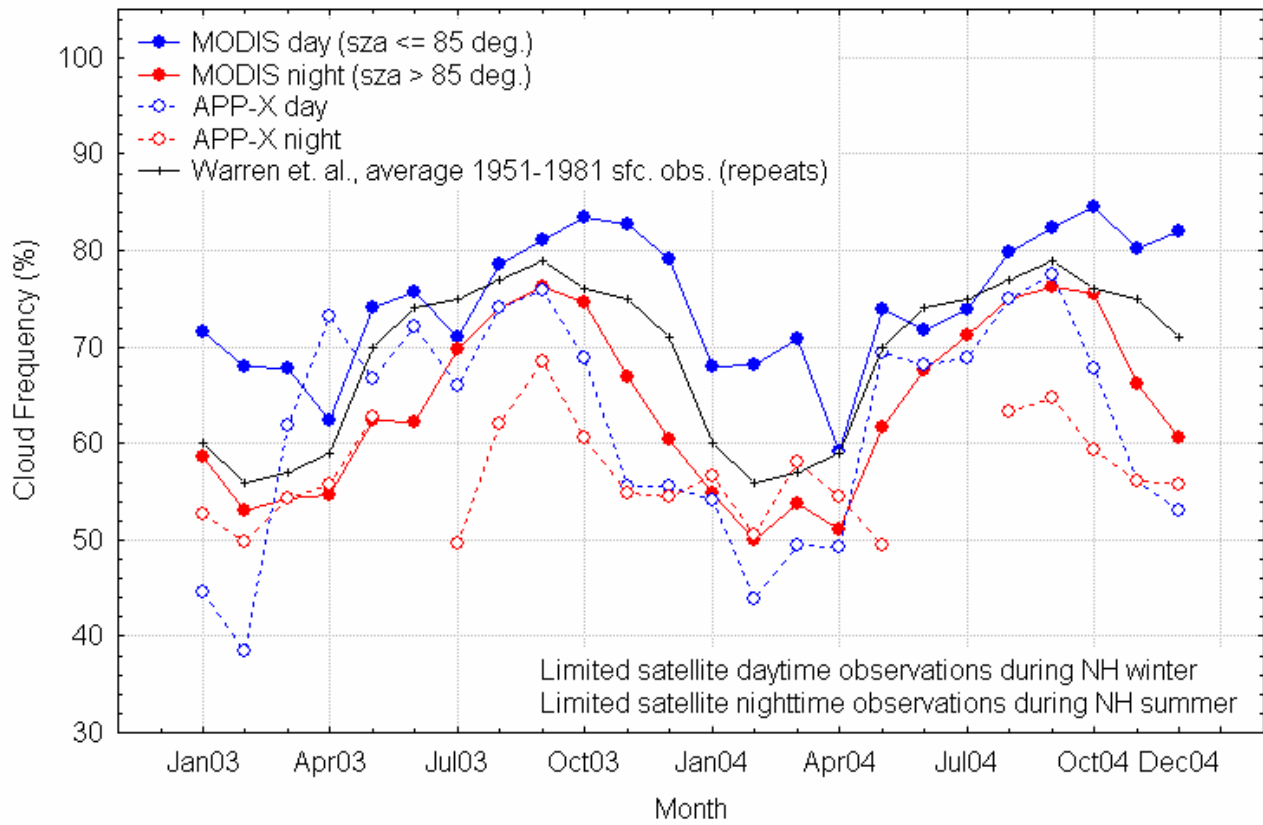


Figure 4. Time series of Aqua MODIS and APP-x Arctic cloud frequencies for day and night conditions from January 2003 through December 2004 (see legend). Warren et al. overall data from 1951-1986 are shown for reference.

Distribution of MODIS vs. APP-X Arctic Cloud Frequencies  
January 2003 - December 2004

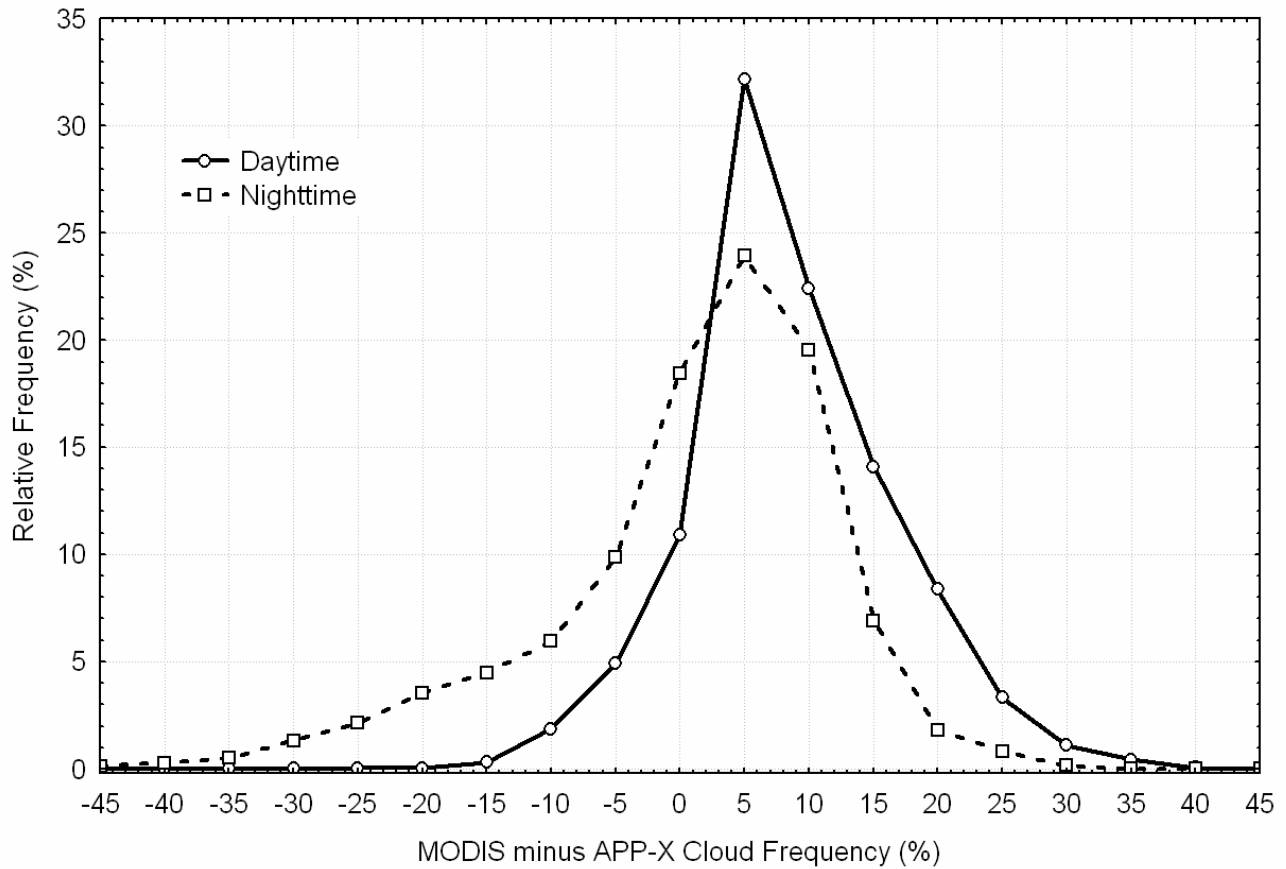


Figure 5. Distributions of cloud frequency differences between Aqua MODIS and APP-x Arctic cloud frequencies for day and night conditions. Time period is January 2003 through December 2004.

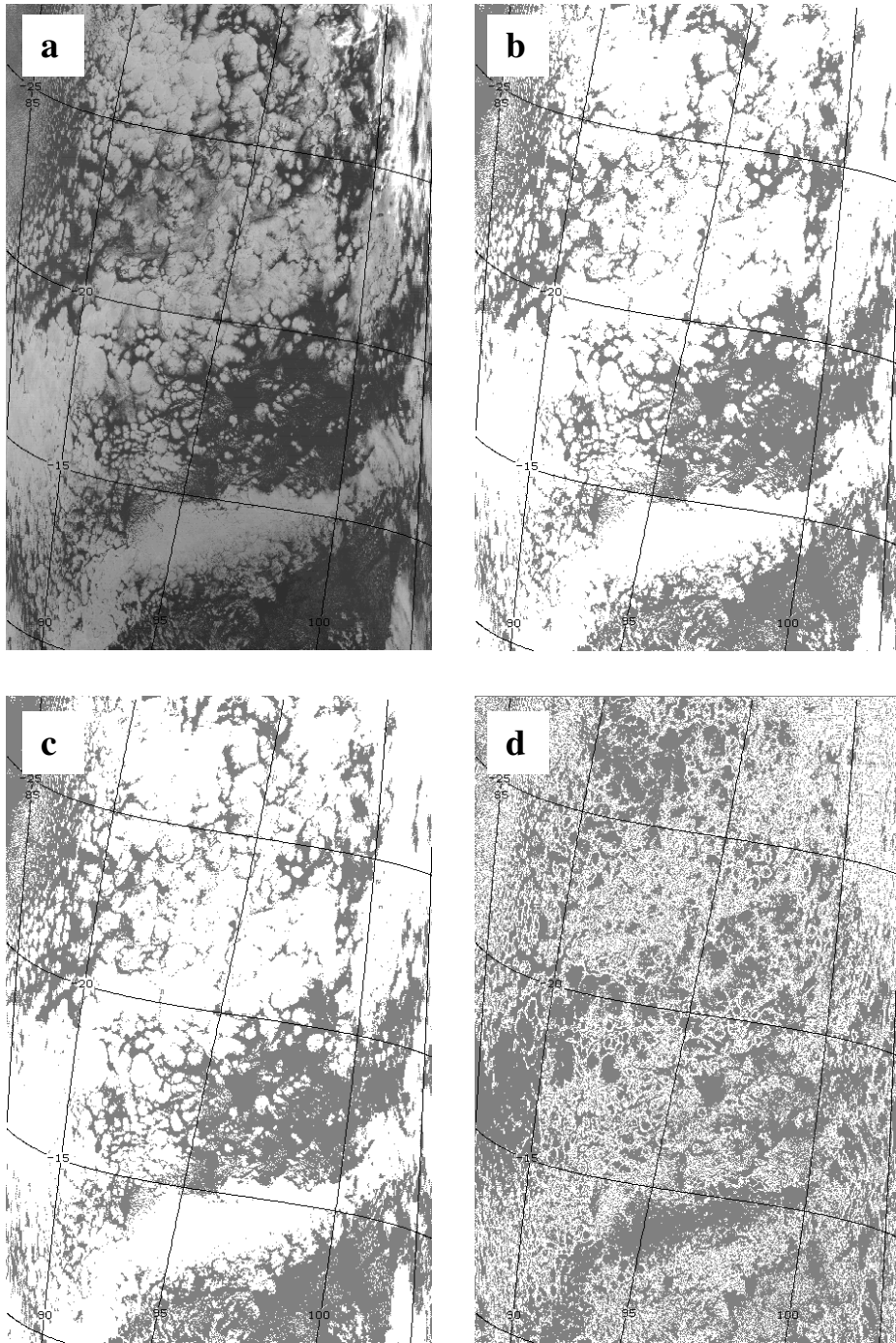


Figure 6. Example scene of a) MODIS 3.9  $\mu\text{m}$  BT image, b) SST test, c) MODIS 8.6-7.2  $\mu\text{m}$  BTD test, and d) 11  $\mu\text{m}$  variability test. Data is from 6 April, 2004 at 19:10 UTC.

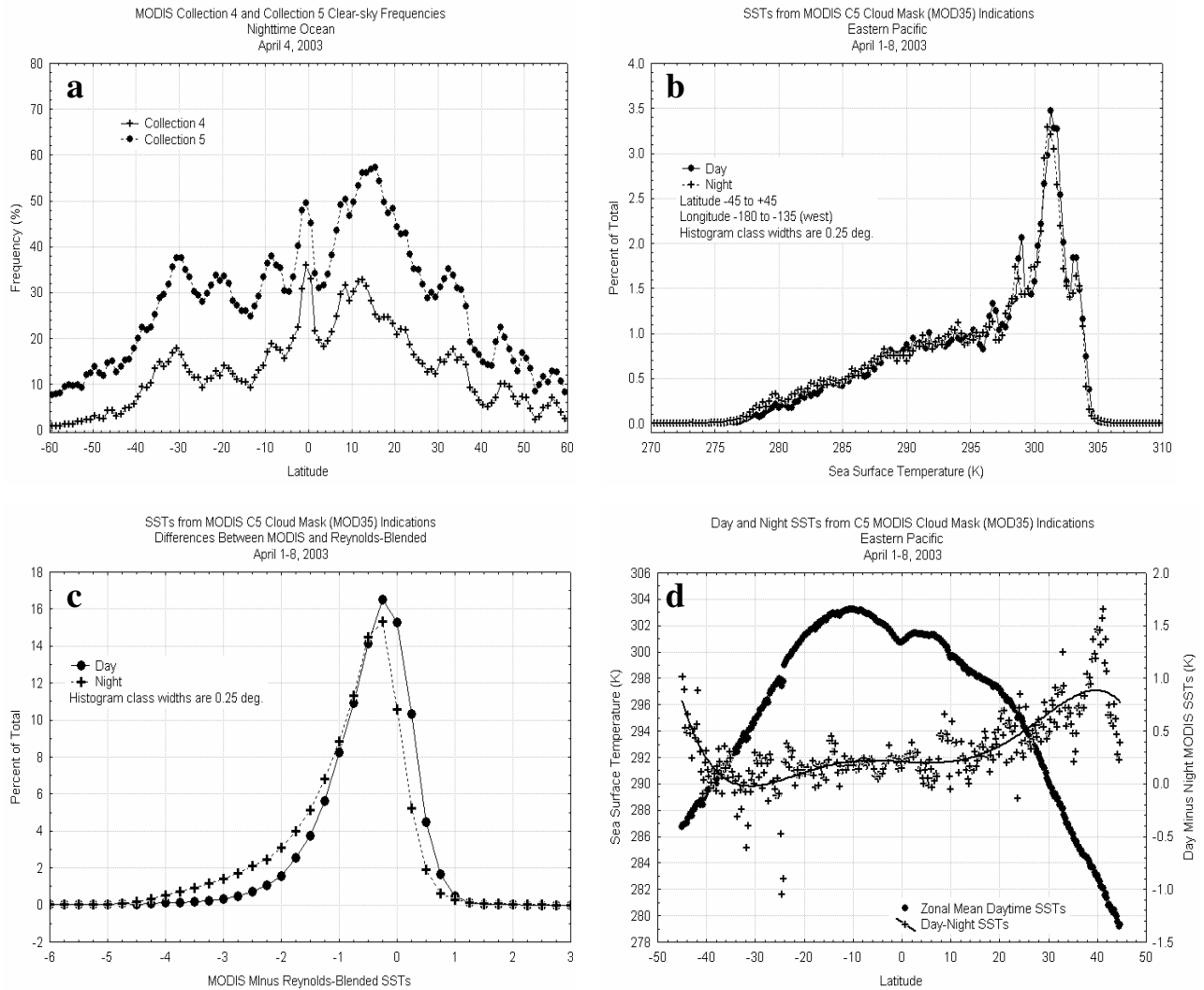


Figure 7. a) zonal mean nighttime ocean clear sky frequency from MODIS Collections 4 and 5 for April 4, 2003, b) histogram of day and night SSTs using the same SST algorithm and coefficients, c) histogram of MODIS versus Reynolds SSTs for day and night, and d) zonal mean daytime SSTs and zonal mean day minus night SSTs. SST analysis uses data from the eastern Pacific Ocean (-45 to +45 latitude and -180 to -130 longitude).

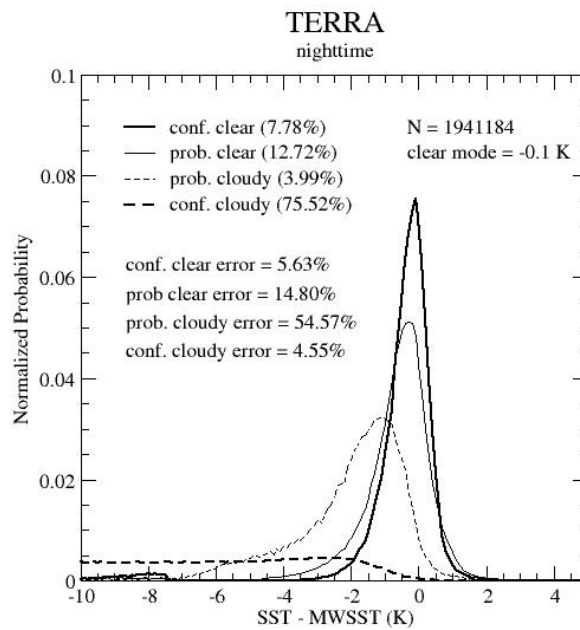
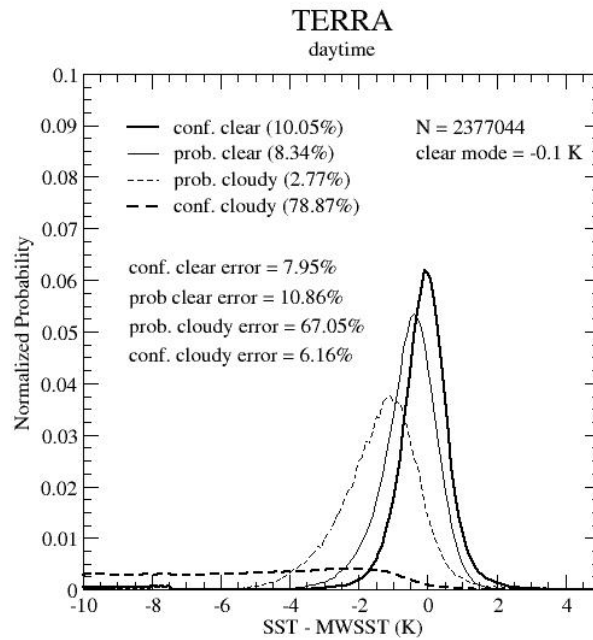


Figure 8. Histograms of MODIS minus MWSST SSTs as functions of MOD35 clear sky confidence levels. Daytime data at top of figure, nighttime at the bottom.

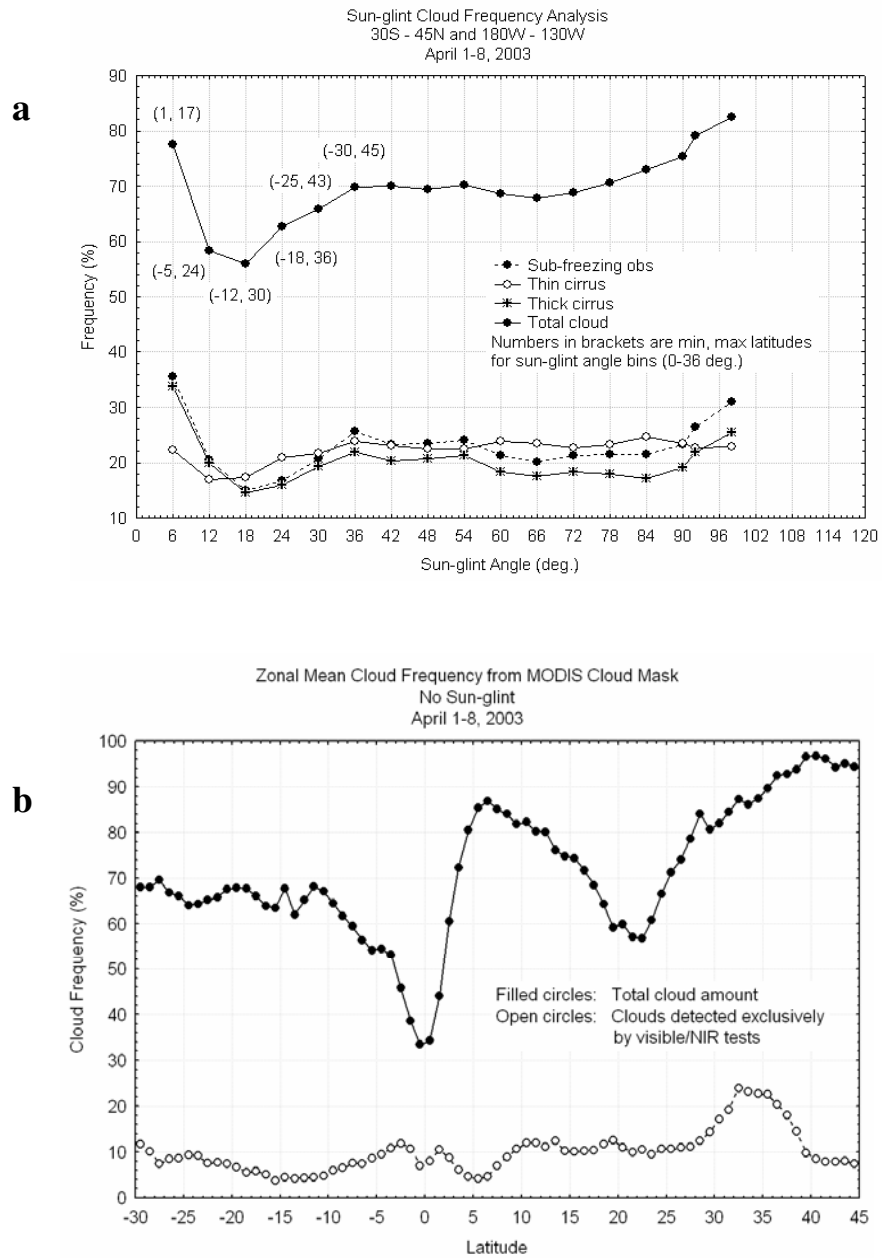


Figure 9. a) cloud frequencies as a function of sun-glint angle, and b) latitude. The cloud frequencies in (b) do not contain any observations from sun-glint conditions. Data is from April 8, 2003.